Mn and Fe doping of bulk Si: Concentration influence on electronic and magnetic properties

F. Küwen,* R. Leitsmann, and F. Bechstedt
Institut für Festkörpertheorie und -optik, Friedrich-Schiller-Universität and European Theoretical Spektroscopy Facility (ETSF), Max-Wien-Platz 1, 07743 Jena, Germany

(Received 4 March 2009; revised manuscript received 15 June 2009; published 10 July 2009)

We investigate the influence of transition-metal doping on silicon crystals by means of *ab initio* first-principles calculations and a supercell approach. We focus on the electronic density of states (DOS) and magnetic moments. Remarkable differences are found between iron and manganese on substitutional positions while interstitial doping leads to similar effects. While the stability of the interstitial position is rather independent of the supercell size and hence the dopant concentration, both concentration and nature of the dopant influence the density of states and the magnetic moments. Magnetic moments seem to be unaffected by iron doping concentration, while they are more sensitive in the manganese case. We observe drastic effects due to the inclusion of strong electron correlation effects.

DOI: 10.1103/PhysRevB.80.045203 PACS number(s): 61.72.Bb, 61.72.uf, 71.55.Cn, 75.50.Pp

I. INTRODUCTION

In recent years there has been a great interest in diluted magnetic semiconductors (DMS). They are supposed to be the materials for new devices, which open the field of spintronics. For instance, spin transistors are devices that can manage spin-polarized currents. In spintronics the switching process is controlled by the spin orientation instead of the charge of the electrons. This allows to build nonvolatile magnetic hard drives. For industrial applications spintronics must conquer silicon; the abundant, inexpensive, and entrenched material of choice for conventional semiconductor electronics.[1] One way could be alloying or doping silicon with transition-metal (TM) atoms such as Mn or Fe.

While there are experimental results on ferromagnetism in Mn_xGe_{1-x} DMS,[2,3] similar results have so far not been reported for Si. However, in addition to germanium[4] there are theoretical suggestions of a new clue for Si-based spintronic materials due to Mn incorporation in alloys[5] and heterostructures[6,7] or TM atom adsorption on Si nanowires.[8] The formation of ferromagnetism due to TM incorporation on the nanometer scale requires a deeper understanding of the TM doping of silicon for various concentrations of the magnetic coupling mechanism of the TM ions, and the effect of electron correlation on the strongly localized TM 3*d* states.

The chemical trends of the TM doping of bulk Si and its influence on electronic energy levels have been studied by self-consistent theoretical methods over the years in detail.[9–12] This holds especially for the consequences of isolated substitutional and interstitial 3*d* impurities. However, the influence of higher doping levels on the electronic and magnetic properties is less studied.[5] In particular, the mechanisms of the formation of a spin ordering versus dopant distance as well as the metallic or nonmetallic character of the doped systems need a deeper understanding. The theoretical studies[4–10] are commonly based on a description of exchange and correlation (XC) effects in the framework of local or semilocal approximations. Typical examples are the applications of the spin-polarized density-functional theory (DFT)[13] within the local-density approximation (LDA)[14] or the generalized gradient approximation (GGA).[15] There are several indications that such approaches do not correctly describe localized electrons in the partially filled 3*d* shells of transition metals. Such strong electron correlation effects beyond the LDA or GGA can be presumably treated by an effective Coulomb interaction U[2] between 3*d* electrons of opposite spin within the so-called LDA+U (or GGA+U) treatment.[16,17]

In the present paper we study the effect of incorporation of Mn and Fe atoms in bulk Si on interstitial and substitutional sites mainly in the framework of a spin-polarized DFT scheme and a supercell approach. The influence of the dopant concentration is simulated by different sizes of the supercells. We visualize the magnetic interaction schemes in the different doping situations via the magnetization densities. Special attention is paid on the effect of exchange and correlation. Therefore, besides the LDA/GGA also the consequences of the inclusion of an effective Coulomb interaction U is investigated.

II. COMPUTATIONAL METHODS

In order to investigate the clean and doped bulk silicon by first-principles techniques we use the density-functional theory in generalized gradient approximation as it is implemented in the Vienna *ab initio* simulation package (VASP).[18] The pseudopotentials are generated by means of the projector-augmented-wave method (PAW)[19] that allows for the accurate treatment of the TM 3*d*, TM 4*s*, Si 3*s*, and Si 3*p* valence electrons. In the region between the atomic cores the wave functions are expanded in plane waves up to a cutoff energy of 200 eV. Usually the XC functional is taken within GGA as parametrized by Perdew and Wang.[15,20] Test calculations are also performed for a LDA functional.[21] For intermediate spin polarizations we use the interpolation scheme proposed by von Barth and Hedin.[22] According to a test investigation the use of another interpolation scheme[23] does not qualitatively change the magnetic moments. Atomic coordinates are obtained by relaxation of the geometry in order to minimize the DFT total energy. Single-particle energies and magnetization densities are derived from the solutions of

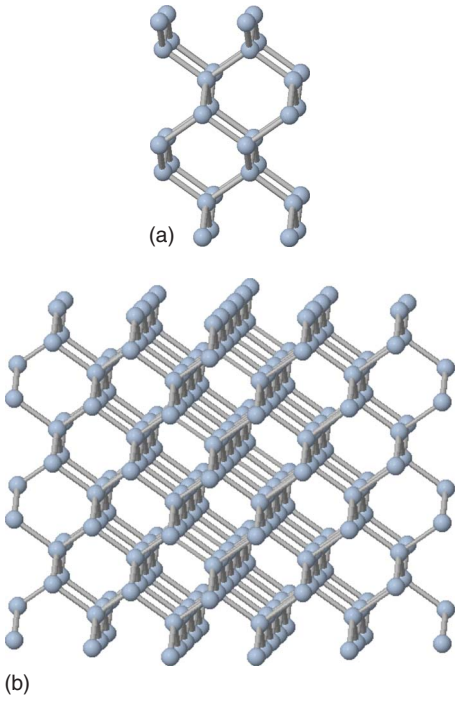

FIG. 1. (Color online) Supercell configuration used for (a) the low-TM concentration $x \approx 0.005$ and (b) the high-TM concentration $x \approx 0.03$. In case of the low-impurity concentration the supercell contains 216 atoms.

the Kohn-Sham (KS) equation for the equilibrium system.

To examine different doping situations we use different types of supercells. The first one represents a high incorporation of transition-metal elements. It is a cell containing 32 Si atoms in the pure silicon case. Its use corresponds to TM_xSi_{1-x} alloys with $x=0.03125$ (substitutional) and $x=0.03030$ (interstitial), i.e., approximately $x=0.03$ [cf. Fig. 1(a)]. The cell and the corresponding tetragonal Bravais lattice are constructed from primitive basis vectors $\boldsymbol{a}_1 = a_0(1,1,0)$, $\boldsymbol{a}_2 = a_0(1,-1,0)$, and $\boldsymbol{a}_3 = 2a_0(0,0,1)$ [cf. Fig. 1(a)] with the bulk cubic lattice constant of about $a_0 = 5.498$ Å (GGA). The point group of the resulting crystal with the arrangement of the TM ions is only a subgroup of that for T_d symmetry. Nevertheless, we still approximately classify the $3d$ states in terms of e_g and t_{2g} symmetries because we expect only a little perturbation of the T_d crystal-field symmetry. To simulate more or less isolated TM dopants we also apply 216-atom supercells with primitive basis vectors $\boldsymbol{a}_1 = 3a_0(1,0,0)$, $\boldsymbol{a}_2 = 3a_0(0,1,0)$, and $\boldsymbol{a}_3 = 3a_0(0,0,1)$ [cf. Fig. 1(b)]. In this arrangement local symmetry around both impurities, interstitial and substitutional, is T_d. The composition amounts to $x=0.004\,63$ and $x=0.004\,61$ (i.e., $x \approx 0.005$). According to our test calculations the magnetic interaction of the TM ions is negligibly small in the case of 216-atom cells.

The reciprocal space summation is restricted to a $5\times5\times5$ mesh for the 216-atom supercell and to $11\times11\times7$ for the 32-atom supercell. The $\boldsymbol{k}$-point meshes for Brillouin-zone (BZ) sampling are generated using the Monkhorst and Pack scheme. The atomic geometries are optimized until the Hellmann-Feynman forces are smaller than 25 meV/Å. Due to slightly different $\boldsymbol{k}$-point densities the cohesive energies per atom μ_{Si} depend on the used supercell. To minimize numerical errors we use, therefore, the value −5.41 eV/atom (32-atom cell) or −5.39 eV/atom (216-atom cell) as chemical potential.

The eigenvalues of the Kohn-Sham equation are used to discuss the electronic structure, especially the density of states (DOS). The corresponding eigenfunctions for the occupied states lead to the magnetization density $m(\boldsymbol{x}) = \mu_B[n_\uparrow(\boldsymbol{x}) - n_\downarrow(\boldsymbol{x})]$, which is mainly represented by the difference in majority-spin and minority-spin densities. Because of the lack of the excitation aspect the KS eigenvalues lead to too small distances between occupied and empty electronic states. The fundamental energy gap of bulk Si $E_g = 0.67$ eV underestimates the experimental gap of about 0.5 eV. This underestimation can be lifted within the quasiparticle picture.[24] The usage of such methods is, however, rather computer-time consuming and yields not really to new physical insights into the electronic and magnetic properties. Therefore, we restrict the studies to the DFT framework without taking the excitation aspect into account.

In order to account for effects of the strong electron correlation on the TM $3d$ shells, we apply the GGA+U method[16] in the approach of Dudarev *et al.*,[17] where only the difference between the on-site Coulomb interaction and the exchange parameter determines the electronic structure. In contrast to earlier suggueststions,[17] a smaller effective U value of 3 eV is used both for Mn and Fe. Recently it has been found that U values in this energy range give rise to the correct ordering of the occupied and empty $3d$-derived e_g and t_{2g} states in antiferromagnetic TM oxides.[25] Larger U values, instead, shift down the occupied Mn $3d$ bands in MnO too much and, hence, to wrong ordering of the bands.[25]

III. ENERGETIC, ELECTRONIC, AND MAGNETIC PROPERTIES DUE TO TM IMPURITY INCORPORATION

A. Energetics and structural consequences

First, we study the stability of the Si bulk doping with Mn and Fe impurities for two different concentrations ($x \approx 0.03$ and $x \approx 0.005$) in the framework of the semilocal GGA for exchange and correlation.[15,21] In the thermal equilibrium the formation energy Ω_f of an impurity depends on the chemical potentials μ_X (X=Si, TM) of the two species according to

$$\Omega_f = \gamma_f - \mu_{TM} N_{TM},$$

$$\gamma_f = E_{tot}(N_{TM}, N_{Si}^*) - E_{tot}(N_{Si}) - \mu_{Si}(N_{Si}^* - N_{Si}), \qquad (1)$$

with the total energies E_{tot} of the doped supercell with N_{TM} (N_{Si}^*) TM (Si) atoms and the pure silicon with N_{Si} atoms in the supercell. The chemical potentials μ_{TM} and μ_{Si} allow us to model different preparation conditions. Since, we only study the incorporation of one TM atom in a supercell, i.e., $N_{TM} \equiv 1$, the influence of the TM reservoir may be neglected. It is sufficient to discuss relative formation energies γ_f.

Their values are given in Table I assuming bulk Si as reservoir. They clearly demonstrate the favorization of the TM incorporation on tetrahedral interstitial sites over the re-

TABLE I. Values for relative formation energy γ_f, magnetic moments of the total cell m_{tot}, and projected onto the TM atom m_{TM} for both supercells and the different TM dopants on both doping sites. We also present the HOMO-LUMO energy gap E_g if the doped system is a semiconductor. Additionally the nearest distance of the TM atom to its surrounding Si neighbors $d_{\mathrm{n.n}}$ is given. The alignment shift is calculated from the electrostatic potential difference ΔV.

Supercell	216 atoms				32 atoms			
Dopant	Mn		Fe		Mn		Fe	
Position	sub.	int.	sub.	int.	sub.	int.	sub.	int.
γ_f [eV]	−6.43	−6.56	−6.33	−6.44	−6.27	−6.67	−5.92	−6.29
m_{tot} [μ_B]	1.02	1.01	0.39	2.03	3.00	3.00	−0.01	2.00
m_{TM} [μ_B]	1.55	1.15	0.02	1.87	2.97	2.59	0.01	1.80
E_g [eV]			0.69	0.50			0.23	0.04
ΔV [eV]	0.02	−0.02	−0.04	0.01	−0.01	−0.015	−0.01	−0.04
$d_{n.n.}$ [Å]	2.32	2.41	2.25	2.41	2.38	2.42	2.27	2.40

placement of a site in the Si lattice. This tendency is enforced for the higher TM concentration from 0.1 toward 0.4 eV. Thereby, the favorization of the tetrahedral interstitial site over the substitutional doping is rather similar for Mn and Fe. The general tendency is in agreement with previous theoretical studies[12,26] and experimental data.[27]

Table I also shows the nearest-neighbor (n.n.) distances $d_{\mathrm{n.n.}}$ between the TM atom and the four Si neighbors. The largest distances $d_{\mathrm{n.n.}}$ somewhat above 2.4 Å are observed for the interstitial sites. Due to the strong covalent bonds these distances $d_{\mathrm{n.n.}}$ are equal or smaller than the bulk Si bond length of 2.38 Å in the substitutional case. The distances Fe-Si are smaller than those for Mn-Si for reasons that will be discussed below.

B. Electronic states

The changes in the electronic structure due to the impurity incorporation are described by the density of states in Figs. 2 and 3 for high and low TM concentrations. For the purpose of comparison also the DOS of pure bulk Si is given (dashed line). The alignment of the energy scales of doped and undoped situations has been made by the electrostatic potentials occurring in the KS equation. The corresponding shifts ΔV (see Table I) are rather small. Only for Fe they approach values of up to 0.04 eV.

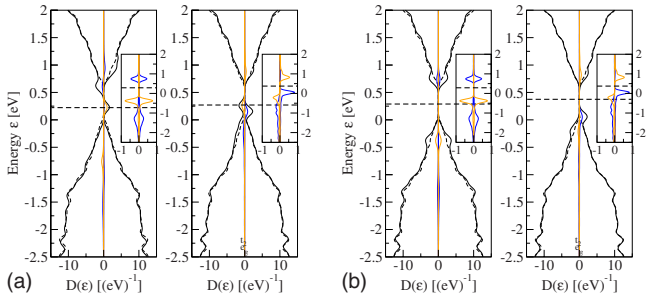

FIG. 2. (Color online) DOS of Si doped with (a) Mn or (b) Fe atoms at substitutional (left panel) or interstitial (right panel) site for low concentration $x \approx 0.005$ (solid line). For comparison DOS of pure Si is also given (dashed line). The t_{2g} (e_g)-projected DOS is plotted as dark blue (light orange) line. The horizontal dashed line indicates the Fermi level. The left (right) part describes the majority (minority)-spin channel. The top of the bulk valence band is taken as energy zero. The insets show the TM 3*d* orbital contribution to the DOS.

In the case of lightly doped Si crystals (Fig. 2) the overall DOS exhibit similarities with that of the pure Si. Only in the energy region around the fundamental gap the electronic structure is substantially changed due to the impurities. It seems to be, especially in the interstitial case, that the level schemes known for Mn and Fe[9] atoms survive. For the interstitial sites there are only small modifications of the t_{2g}-derived *d* states due to their hybridization with the neighboring Si sp^3 orbitals and the formation of bonding and antibonding combinations. In the substitutional case the sequence of the bonding t_{2g} levels, e_g levels, and antibonding t_{2g} levels is observed independent of the spin channel. However, while for Fe these levels possess almost the same energy, the majority-spin channel levels are lowered in energy for Mn. In the interstitial case the sequences $t_{2g\uparrow}$, $e_{g\uparrow}$, $t_{2g\downarrow}$, and $e_{g\downarrow}$ (Fe) and $t_{2g\uparrow}$, $t_{2g\downarrow}$, $e_{g\uparrow}$, and $e_{g\downarrow}$ (Mn) are observed. These results with respect to the level ordering are almost in agreement with previous[9] and very recent[12] results. Discrepancies mainly occur for the substitutional impurities compared with former studies.

The two dopants act differently with respect to the conductivity of the doped silicon resulting within the DFT-GGA

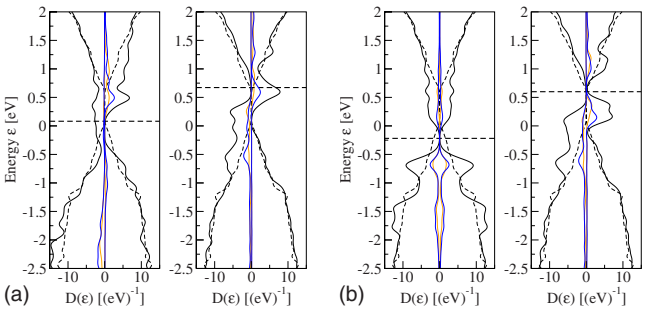

FIG. 3. (Color online) As in Fig. 2 but for the high-TM concentration $x \approx 0.03$.

framework. While Mn doping yields a half-metallic character independent of the doping site, Fe-doped silicon is an insulator. These findings are in agreement with the odd (even) number of the $3d$ electrons of Mn (Fe). The half metallicity of Mn-doped silicon is caused by half-filled $e_{g\downarrow}$ ($e_{g\uparrow}$) levels for substitutional (interstitial) doping situation.

In the substitutional case and low-doping concentrations [(Figs. 2(a) and 3(b)), left panel] the level orderings and occupations can be explained within a simple defect-molecule model taking the TM $4s$, TM $3d$, and Si sp^3 orbitals into account.[28] The $a_{1\uparrow}$ and $a_{1\downarrow}$ bonding combinations in the valence-band region are occupied. The same holds for the $t_{2g\uparrow}$ or $t_{2g\downarrow}$ bonding combination near the top of the valence bands. The nonbonding e_g levels in almost midgap positions are completely filled (Mn $e_{g\uparrow}$, Fe $e_{g\uparrow}$, and Fe $e_{g\downarrow}$) or only partially filled (Mn $e_{g\downarrow}$). Therefore the Mn $e_{g\downarrow}$ states pin the Fermi level. For Fe doping, a gap E_g between the lowest unoccupied molecule orbital (LUMO), the antibonding $t_{2g\uparrow/\downarrow}$ levels, and the highest occupied molecule orbital (HOMO), the nonbonding $e_{g\uparrow/\downarrow}$ levels, appears. In the interstitial case indeed TM-free-atom-derived states governs the DOS changes near the fundamental gap. However, the occupation is changed. The $t_{2g\uparrow}$ and $t_{2g\downarrow}$ levels are occupied, while the $e_{g\downarrow}$ level remains empty. The $e_{g\uparrow}$ level is filled (half occupied) for Fe (Mn).

The dopant modification of the DOS is much bigger in the high-concentration limit $x \approx 0.03$ [cf. Figs. 3(a) and 3(b)]. This is the result of the interaction of neighboring TM atoms in distances of 0.8–1.0 nm and, in addition, also due to their magnetic interactions. Apart from the level shifts due to the strong impurity-impurity interaction, the impurity levels in the gap region are broadened to impurity bands resulting in broader features in the DOS except of an iron atom at substitutional site. The projection onto t_2 states and atomic sites demonstrates that the broad structures are related to Si states localized at neighboring atoms. They pin the Fermi level in the majority-spin channel of the substitutional Mn. In contrast to the low-doping situation the half-metallic character of silicon doped with interstitial Mn is now due to the Fermi level pinning by a broad, strongly $t_{2g\downarrow}$-related feature, with consequences for their spin state and the magnetization. In general, due to the broadening effects, it is more difficult to relate the structural features to certain localized states.

C. Magnetization densities and magnetic moments

The computed magnetization densities $m(\boldsymbol{x})$ are plotted in Figs. 4 and 5 in a (110) plane containing the zigzag chains of Si-Si bonds. The resulting magnetic moments m_{tot} of a supercell and those of a TM atom m_{TM} (integrated over space of the half nearest-neighbor distances $d_{\mathrm{n.n.}}$) are listed in Table I. Comparing Figs. 4 and 5 one observes the strongest changes in the magnetization density with the doping concentration for Mn. The different magnetic densities for substitutional Mn in Figs. 4 and 5 characterize the changes from an isolated magnetic atom to an interacting array of transition-metal atoms. In the low-concentration limit, Mn doping gives rise to a total magnetic moment $m_{tot}=1\ \mu_B$ independent of the impurity site. Independent of the doping

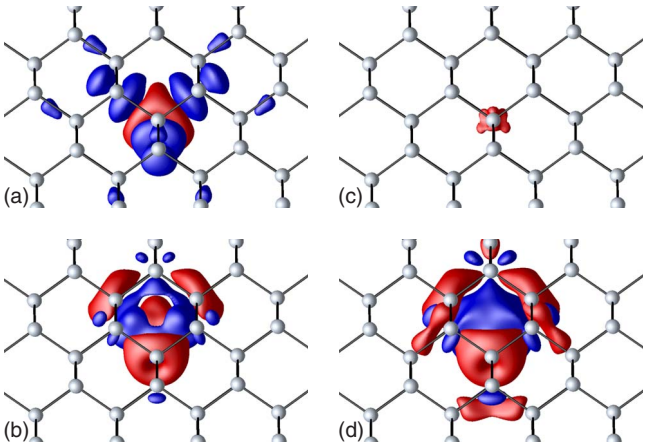

FIG. 4. (Color online) Magnetization density in a (110) plane for (a) and (b) Mn and (c) and (d) Fe doping with low concentration $x \approx 0.005$. (a) and (c) Substitutional and (b) and (d) interstitial positions are studied. The isosurface corresponds to a density of 2.5×10^{-3} Å^3. Light red (dark blue) color indicates the excess of majority (minority)-spin density.

site, in the high TM concentration case, Mn occurs in the high-spin state with $m_{tot}=3\ \mu_B$ in agreement with theoretical and experimental findings in the literature.[9,12] The reason is the change in the symmetry ($e_{g\downarrow} \rightarrow t_{2g\downarrow}$) and the degeneracy of the level that leads to the half metallicity. The magnetization densities for Fe in silicon are rather similar for the two discussed doping concentrations. Consequently the magnetic moments remain almost unchanged, $m_{tot}=0.4 \ldots 0.0\ \mu_B$ (substitutional Fe) and $m_{tot}=2\ \mu_B$ (interstitial Fe), with values close to the findings in the literature.[9]

The strong changes in the magnetic properties with the distance of the Mn atoms in the Si host and the remaining half metallicity suggest a Ruderman, Kittel, Kasuya, and Yosida mechanism (RKKY).[29–32] The spin degeneracy of the localized levels of the isolated TM impurities is lifted through the crystal field of the host material and the majority (minority)-spin impurity levels are below (above) the Fermi energy. This leads to a magnetic moment of this half metal which polarizes the spins of the electrons in the surrounding

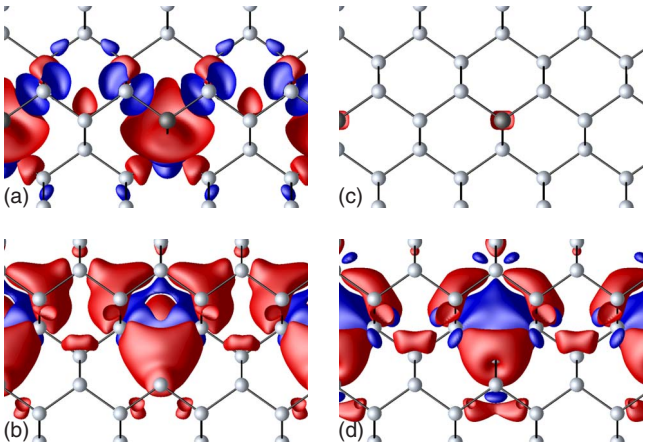

FIG. 5. (Color online) As in Fig. 4 but for high-doping concentrations $x \approx 0.03$.

bonds of the half metal with the result that the probability density is more or less unchanged for the bonds but with an oscillation of the spin orientation (Friedel oscillation). The insulating character of Fe-doped silicon suggests another interacting mechanism, e.g., the Zener mechanism.[33] In the Zener model of double exchange the magnetic moment interacts across a diamagnetically bonded atom between the magnetic atoms. An electron mediates between magnetic interactions through two simultaneous transfer processes from the first magnetic atom to the other along the diamagnetic bond. Characteristic of such kind of an interaction is an insulating character of the host material and anisotropic spin-orbit coupling. The electrons are transferred from the crystal states to the impurity states which are the origin of the magnetism.[34] In our systems the *d* states of the transition-metal atoms interact strongly with the surrounding sp^3 states (cf. Fig. 2). It is a similar effect as reported in the literature based on the *p-d* exchange.[35–37]

IV. EFFECT OF COULOMB CORRELATION

In order to discuss the question whether the semilocal description of exchange and correlation is still reasonable for the TM 3*d* electrons we repeated the electronic structure and magnetization calculations in the framework of the GGA $+U$ method.[16,17,38,39] With respect to the resulting magnetic properties the description of the strong repulsion of electrons with opposite spin by the U parameter may also be interpreted as the application of the Stoner model for the exchange operater.[40] The studies have been done for both TM impurity concentrations (or supercells) of interest. Nevertheless, we only present and discuss the results obtained for TM impurities in a 216-atom supercell with $x \approx 0.005$ (Fig. 6) because the effect can be more clearly seen for a localized magnetic moment. The observed low-spin (high-spin) state for Mn in Si for lower (higher) impurity concentrations let expect a higher sensitivity of the Coulomb correlation U on the more isolated Mn impurities. Indeed, Mn in Si within the small 32-atom supercell ($x \approx 0.03$) (no figures shown), remains a half metal independent of the doping site. The magnetic moments $m_{tot} \approx 3\ \mu_B$ are practically not changed. The same holds for interstitial Fe. However, a drastic change from $m_{tot} \approx 0\ \mu_B$ to $m_{tot} \approx 4\ \mu_B$ is found for substitutional Fe. The corresponding high-spin state is connected with the half-metallic character of the system. Despite the significant shift in the *d* levels toward lower energies in the majority-spin channel and a small one for the minority-spin channel in the opposite direction, states appear at the Fermi level close to Si sp^3 orbitals localized at the atomic neighbors.

The results for the change in the DOS with the strong electron correlation characterized by the $U=3$ eV parameter are presented in Fig. 6 for low concentrations of Mn and Fe impurities at substitutional and interstitial sites. The Mn-doped silicon [Figs. 6(a) and 6(b)] keeps its half-metallic character for different reasons. In general, 3*d*-derived states are shifted toward lower (higher) energies in the majority (minority)-spin channel in agreement with their occupation according to $U(\frac{1}{2}-n)$ ($n=0,1$ as the level occupation).[17] The Fermi level is not anymore pinned by $e_{g\downarrow}$ (substitutional) or

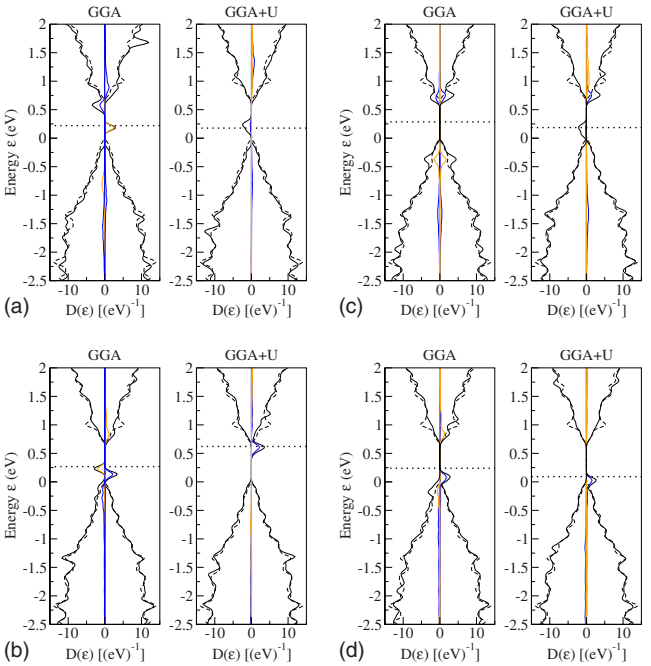

FIG. 6. (Color online) DOS (solid line) of Si doped with (a) and (b) Mn or (c) and (d) Fe on (a) and (c) substitutional and (b) and (d) interstitial sites in the low-concentration limit (216-atom supercell). The t_{2g} (e_g)-projected DOS is plotted as dark blue (light orange) line. The horizontal dashed line indicates the Fermi level. The top of the bulk valence bands is taken as energy zero. Spectra without (left panel) and with (right panel) strong electron correlation are compared.

$e_{g\uparrow}$ (interstitial) states. Rather, Si sp^3 combinations with t_{2g} symmetry character pin the Fermi level for substitutional Mn, while for interstitial Mn the $t_{2g\downarrow}$-derived states and hence the Fermi level are shifted toward the bottom of the conduction bands. Simultaneously, the magnetic moment is increased from $m_{tot}=1\ \mu_B$ to $m_{tot}=3\ \mu_B$ for both doping sites. This agrees with the spin value $S=\frac{3}{2}$ measured for neutral interstitial Mn.[9] However, the value $S=1$ measured for substitutional Mn^+ also seems to fit (interpolating to the neutral case) to the $m_{tot}=3\ \mu_B$ prediction for the neutral defect.

At the first glance the effect of the strong electron correlation on the DOS of Si with Fe impurities in Figs. 6(c) and 6(d) seems to be negligible, since the insulating character is conserved. However, apart from the drastic redistribution of e_g states, in general, also the level scheme is changed for substitutional Fe. First, the spin degeneracy is lifted. Second, due to the significant shifts in the *d*-derived levels only one 3*d*-related DOS peak remains near the valence-band maximum. The corresponding states are essentially built by t_{2g} combinations of Si sp^3 orbitals. The magnetic moment increases from $m_{tot}=0.4\ \mu_B$ to $m_{tot}=4\ \mu_B$. The effect may be described within a Stoner model.[40] In any case it shows that strong similarities with the Mn case on the same doping site are inherent in the gap region of the DOS. The DOS change for interstitial Fe is comparably small and the magnetic moment is conserved at $m_{tot}=2\ \mu_B$ in agreement with experimental and theoretical values in the literature.[9,27,41]

V. SUMMARY AND CONCLUSIONS

The incorporation of Mn and Fe impurities in silicon crystals has been studied in the framework of the *ab initio* density-functional theory for two different descriptions of the exchange-correlation functional, within GGA and GGA+U. For the neutral defects, the consequences of the doping positions and the accompanying chemical bonding have been studied for the electronic structure, especially the density of states, and the magnetic moments.

In general, the interstitial position is favored over the substitutional doping site. Thereby, the differences in the formation energies are increased with doping concentration within GGA. The magnetic moments of $m_{tot}=1$ (sub. Mn), 1 (int. Mn), 0 (sub. Fe), and 2 μ_B (int. Fe) are in agreement with previous theoretical findings. For a reduced interaction of the impurity atoms, i.e., for lower concentrations, these values are almost conserved for Fe, while for Mn one computes $m_{tot}=1$ μ_B, i.e., a low-spin state, within the DFT-GGA framework.

The strong electron correlation characterized by an effective Coulomb interaction U helps to stabilize the high-spin states. Consequently, a magnetic moment of $m_{tot}=3\mu_B$ is found for both substitutional and interstitial Mn. However, a dramatic effect occurs for substitutional Fe with a resulting $m_{tot}=4$ μ_B. The reason is that the electronic configurations in the majority-spin and minority-spin channels giving rise to the global magnetic moments are drastically changed by pushing d states away from the fundamental gap. Simultaneously, the role of spin-polarized t_{2g} combinations of Si sp^3 states localized at the nearest neighbors has been increased. Summarizing the results, one may conclude that strong electron correlation effects are important for the impurity positions for all doping situations. However, it is especially important for the magnetic properties because the finite U tends to transform the system in a high-spin state if possible.

ACKNOWLEDGMENTS

We gratefully acknowledge helpful discussion with C. Rödl and J. Furthmüller. Financial support was provided by the Fonds zur Förderung der Wissenschaftlichen Forschung (Austria) via Grant No. SFB25 IR-ON and by Deutsche Forschungsgesellschaft (Project No. Be 1346/20-1). We thank the Leibniz Rechnenzentrum München and the HLRS in Stuttgart for computer time.

*Present address: LaserAnwendungsCentrum, Technische Universität Clausthal, Am Stollen 19, 38640 Goslar, Germany.

[1] I. Žutić and J. Fabian, Nature (London) **447**, 268 (2007).
[2] Y. D. Park, A. Wilson, A. T. Hanbicki, J. E. Mattson, T. Ambrose, G. Spanos, and B. T. Jonker, Appl. Phys. Lett. **78**, 2739 (2001).
[3] Y. D. Park, A. T. Hanbicki, S. C. Erwin, C. S. Hellberg, J. M. Sullivan, J. E. Mattson, T. F. Ambrose, A. Wilson, G. Spanos, and B. T. Jonker, Science **295**, 651 (2002).
[4] Y.-J. Zhao, T. Shishidou, and A. J. Freeman, Phys. Rev. Lett. **90**, 047204 (2003).
[5] A. Stroppa, S. Picozzi, A. Continenza, and A. J. Freeman, Phys. Rev. B **68**, 155203 (2003).
[6] M. C. Qian, C. Y. Fong, K. Liu, W. E. Pickett, J. E. Pask, and L. H. Yang, Phys. Rev. Lett. **96**, 027211 (2006).
[7] H. Wu, P. Kratzer, and M. Scheffler, Phys. Rev. Lett. **98**, 117202 (2007).
[8] E. Durgun, D. Cakir, N. Akman, and S. Ciraci, Phys. Rev. Lett. **99**, 256806 (2007).
[9] F. Beeler, O. K. Andersen, and M. Scheffler, Phys. Rev. B **41**, 1603 (1990).
[10] A. Zunger and U. Lindefelt, Phys. Rev. B **27**, 1191 (1983).
[11] H. Katayama-Yoshida and A. Zunger, Phys. Rev. B **31**, 8317 (1985).
[12] Z. Z. Zhang, B. Partoens, K. Chang, and F. M. Peeters, Phys. Rev. B **77**, 155201 (2008).
[13] P. Hohenberg and W. Kohn, Phys. Rev. **136**, B864 (1964).
[14] W. Kohn and L. J. Sham, Phys. Rev. **140**, A1133 (1965).
[15] J. P. Perdew, *Electronic Structure of Solids '91* (Akademie Verlag, Berlin, 1991), p. 11.
[16] V. I. Anisimov and O. Gunnarsson, Phys. Rev. B **43**, 7570 (1991).
[17] S. L. Dudarev, G. A. Botton, S. Y. Savrasov, C. J. Humphreys, and A. P. Sutton, Phys. Rev. B **57**, 1505 (1998).
[18] G. Kresse and J. Furthmüller, Comput. Mater. Sci. **6**, 15 (1996).
[19] G. Kresse and D. Joubert, Phys. Rev. B **59**, 1758 (1999).
[20] J. P. Perdew and Y. Wang, Phys. Rev. B **45**, 13244 (1992).
[21] J. P. Perdew and A. Zunger, Phys. Rev. B **23**, 5048 (1981).
[22] U. von Barth and L. Hedin, J. Phys. C **5**, 1629 (1972).
[23] S. H. Vosko, L. Wilk, and M. Nusair, Can. J. Phys. **58**, 1200 (1980).
[24] W. G. Aulbur, L. Jönsson, and J. W. Wilkins, Solid State Phys. **54**, 1 (2000).
[25] C. Rödl, F. Fuchs, J. Furthmüller, and F. Bechstedt, Phys. Rev. B **77**, 184408 (2008).
[26] S. Yabuuchi, E. Ohta, H. Kageshima, and A. Taguchi, Physica B **376-377**, 672 (2006).
[27] D. A. von Wezep and C. A. J. Ammerlaan, J. Electron. Mater. **14**, 863 (1985).
[28] R. Enderlein and N. J. M. Horing, *Fundamentals of Semiconductor Physics and Devices* (World Scientific, Singapore, 1997).
[29] M. A. Ruderman and C. Kittel, Phys. Rev. **96**, 99 (1954).
[30] K. Yosida, Phys. Rev. **106**, 893 (1957).
[31] J. H. Van Vleck, Rev. Mod. Phys. **34**, 681 (1962).
[32] C. Kittel, *Introduction to Solid State Physics* (Wiley, New York, 2005).
[33] C. Zener, Phys. Rev. **82**, 403 (1951).
[34] T. Dietl, H. Ohno, F. Matsukura, J. Cibert, and D. Ferrand, Science **287**, 1019 (2000).
[35] K. Sato and H. Katayama-Yoshida, Semicond. Sci. Technol. **17**, 367 (2002).
[36] K. Sato, P. H. Dederichs, and H. Katayama-Yoshida, Europhys. Lett. **61**, 403 (2003).
[37] K. Sato, P. H. Dederichs, H. Katayama-Yoshida, and J.

Kudrnovsky, J. Phys.: Condens. Matter **16**, S5491 (2004).
[38] K. Sato, P. H. Dederichs, and H. Katayama-Yoshida, Physica B **376-377**, 639 (2006).
[39] M. Toyoda, H. Akai, K. Sato, and H. Katayama-Yoshid, Physica B **376-377**, 647 (2006).
[40] E. C. Stoner Proc. R. Soc. London **169**, 339 (1939).
[41] A. A. Istratov, H. Hieslmair, and E. R. Weber, Appl. Phys. A **69**, 13 (1999).